INTERNATIONAL JOURNAL FOR NUMERICAL AND ANALYTICAL METHODS IN GEOMECHANICS
Int. J. Numer. Anal. Meth. Geomech. 2014; **38**:236–255
Published online 5 July 2013 in Wiley Online Library (wileyonlinelibrary.com). DOI: 10.1002/nag.2202

Layout design of rockbolts for natural ground reinforcement

Junji Kato[1,*,†], Keiichiro Ishii[2], Kenjiro Terada[1] and Takashi Kyoya[2]

[1]*International Research Institute of Dissaster Sceience, Tohoku University, Aramaki-Aoba 6-6-06, Aoba, Sendai, 980-8579, Japan*
[2]*Mechanics of Materials Laboratory, Tohoku University, Aramaki-Aoba 6-6-06, Aoba, Sendai, 980-8579, Japan*

SUMMARY

The present study addresses a layout design of rockbolts for reinforcing natural ground structures applying a special optimization method, called *multiphase layout optimization*. Rockbolts are used to tighten loosed natural ground, and the layout of rockbolts are determined without sufficient information about the physical properties of the ground materials. Because of this uncertainty, unexpected deformation often occurs at the excavation surface of natural ground. In that case, it is requested to determine an effective layout of the additional rockbolts promptly with respect to the actual deformation at the construction site. However, it is not easy to determine the optimal layout because of its complexity, and consequently, it has no choice but to determine the layout in an empirical way.

This study introduces a numerical approach to determine an optimal layout of rockbolts with respect to arbitrarily possible deformation of natural ground. The objective is to maximize the stiffness of the overall ground structure reinforced with rockbolts. For optimization, a gradient-based optimization scheme is applied because of its numerical efficiency. It was verified from a series of numerical examples that this method has great potential to improve the stiffness of the overall ground structure and shows a certain applicability to a practical design. Copyright © 2013 John Wiley & Sons, Ltd.

Received 13 February 2013; Revised 28 April 2013; Accepted 29 April 2013

KEY WORDS: multiphase layout optimization; rockbolts; reinforcement; NATM; reinforced slopes

1. INTRODUCTION

Rockbolt tunnel support has been widely employed in the New Austrian Tunneling Method (NATM), the representative construction method for building tunnels. The mechanism for reinforcing natural ground is to integrate the ground by the tensile strength of rockbolts cast into the ground and to increase the stiffness of the integral structure to prevent collapse of the natural ground.

Although much experience has been accumulated with rockbolt tunnel support, the problem in designs is how to determine the layout of the rockbolts without sufficient information about the physical properties of the ground material. For instance, with regard to the NATM, as it is difficult to obtain the material properties of natural ground that stands apart from the reclaimed surface, the usual method for determining the layout is to roughly classify the natural ground by using the insufficiently known physical properties of the ground materials and then to choose the most suitable layout pattern for the conditions from the standard layout patterns of tunnel support systems determined by past experience and performance. In the layout patterns, called 'the standard layout patterns of tunnel support system', the rockbolts are cast into natural ground with the same length, placed radially with equal spacing, and are said to present an effective layout against isotropic ground pressure.

*Correspondence to: Junji Kato, International Research Institute of Dissaster Sceience, Tohoku University, Aramaki-Aoba 6-6-06, Aoba, Sendai, 980-8579, Japan.
†E-mail: jkato@civil.tohoku.ac.jp

However, the stress condition of the natural ground during excavation of the tunnel is rather subjected to anisotropic ground pressure because of the influences of the initial ground pressure before digging, biased ground pressure from the surrounding geography, strength and discontinuous surfaces of the bare rock, and furthermore, from ground water. For instance, tunnels with comparably less overburden will be dominated by vertical ground pressure, and large cross-section tunnels tend to be dominated by the stress from the sides and from underneath. Furthermore, unexpected deformation at the excavation surface often appears because of these anisotropic pressures at an actual excavation site. In that case, additional casting of rockbolts is necessary to reduce the deformation. However, it is not easy to find out the cause of the deformation and to determine promptly the effective layout of rockbolts at the construction site in reality. Consequently, the layout of the additional rockbolts is determined by an empirical approach, which may not be mechanically effective. For this reason, it has been expected to develop a system that enables to numerically determine an optimal layout of rockbolts with respect to arbitrarily possible deformation of natural ground. Of course, this system will be applicable not only for tunnel support systems but also for other reinforcement works, such as reinforcing slopes.

The purpose of this study is to introduce a numerical approach to determine an optimal layout of rockbolts with respect to arbitrarily possible deformation of natural ground. The objective is to maximize the stiffness of the integrated structure of natural ground including rockbolts for reinforcement works. The present study solves this problem by structural optimization using a finite element method. One of the difficulties in this approach for our problem is how to discretize the domains of rockbolts and natural ground simultaneously. Thickness of a rockbolt is very thin compared with the size of natural ground; this results in a very complex and fine finite element mesh when a general finite element is employed. To resolve the difficulty, we apply a special numerical approach called 'multiphase layout optimization' [1, 2].

Multiphase layout optimization has been developed to simultaneously optimize type, thickness, and layout (overall design) of fiber reinforcement to improve stiffness and toughness of fiber-reinforced composites. One of the features of the method is to discretize the fiber reinforcement by using special finite element called an embedded reinforcement element [3–8], by which it is possible to build composite material models with highly realistic mechanical behavior and to easily handle alteration of the layout of the reinforcement.

This study determines the most appropriate layout of rockbolts, by substituting rockbolts for the fiber reinforcement and by changing the thickness and length of the rockbolts. To accurately reflect the mechanical behavior of the natural ground and rockbolts, it is necessary to build three-dimensional structure models considering influence by cracks in the natural ground, evaluation of the strength, slippage between rockbolts and the natural ground, or materially nonlinear behavior of mortar to be filled in between a rockbolt and the natural ground. However, as this study is at the basic stage of applying the multiphase layout optimization to the layout of rockbolts, we use a linear elastic material model for simplification and in addition, limit to two-dimensional plane problem. Also, we exclude the influence of shotcrete (sprayed concrete) and assume ideal conditions with no slippage between rockbolt and the natural ground.

In the following section, we simply explain the finite element formulation by using the multiphase layout optimization and embedded reinforcement element. Then we describe the optimization problems for this study and the process of deriving the sensitivity. With regard to the method to solve the optimization problem, a gradient-based method is employed along with a method of moving asymptotes [9–11], which is robust and reliable for numerical analysis. Finally, the possibility of application for actual design is verified by a series of numerical examples, where not only the layout optimization of rockbolts for the NATM but also for reinforcing slopes are demonstrated as an example of other reinforcement works.

2. MULTIPHASE LAYOUT OPTIMIZATION

2.1. Outline

Structural optimization is a method to improve mechanical behavior of a structure by minimizing or maximizing the values of an objective function, defined for mechanical performance such as stiffness

DOI: 10.1002/nag

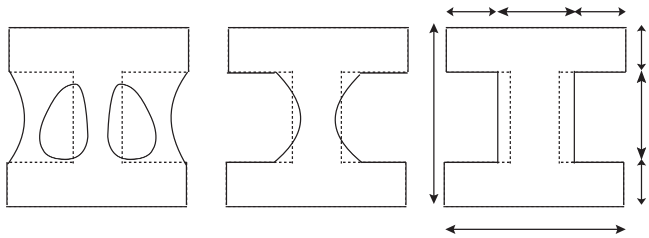

Figure 1. Classification of structural optimization: (a) topology optimization, (b) shape optimization, and (c) size optimization.

of a structure, loading capacity, and natural frequency, using the numerical approach. Structural optimization can be generally classified into three categories as shown in Figure 1. Topology optimization is to determine the topology of the structure; shape optimization is to determine the outer or inner shape of a structure by preserving the topology; and size optimization is to determine the most appropriate dimensions of the constituent parts. Each relates to the geometry of a structure.

On the other hand, there is an additional category of material optimization, which is to determine the optimal types and layouts of constituents. Multiphase layout optimization [1, 2] is one of the material optimization methods and can simultaneously optimize the types, thickness, and global layout of the fiber reinforcement to improve the toughness and stiffness of fiber-reinforced composites, as previously mentioned. The method is a combination of multiphase material optimization [12] and material shape optimization [13]; the former optimizes the types and thickness of the fiber reinforcement, and the latter optimizes global layout including the curve profile. The present study substitutes rockbolts for the reinforcement and handles their length and thickness in 2D as the variables.

In this paper, we give a brief outline of multiphase material optimization and material shape optimization and would like to refer the reader to the literature [12, 13] for further reading on the details thereof.

Superscripts such as $(\bullet)^{\mathrm{r}}$ and $(\bullet)^{\mathrm{b}}$ used in this paper mean the terms of natural ground and rockbolts, respectively. Also, simplified expressions such as $(\bullet)^{\mathrm{r+b}} = (\bullet)^{\mathrm{r}} + (\bullet)^{\mathrm{b}}$ are used. Subscripts such as $(\bullet)_{\mathrm{L}}$ and $(\bullet)_{\mathrm{G}}$ denote the values of axial directions of the rockbolts defined by the local and global coordinate system respectively, but $(\bullet)_{\mathrm{G}}$ will be omitted for simplicity unless special necessity arises.

2.2. *Multiphase material optimization*

This section introduces a two-phase material optimization. The present methodology is strongly related to topology optimization, in particular to the *Solid Isotropic Microstructure with Penalization of intermediate densities* for a one-phase material, the so-called SIMP approach [14], [15], and to its generalization to multiphase topology optimization [16], for example, used for composite structures.

In the SIMP approach, normalized density (porosity) ρ/ρ_0 $(0 \leqslant \rho/\rho_0 \leqslant 1)$ is taken as the design variable, and the intermediate densities are used as mathematical vehicle to relax the ill-posed problem during optimization, see Figure 2 (a). The exponent η plays the role of a penalization factor without a physical meaning eventually leading to a pure or at least an almost pure 0–1 layout for a single material structure as depicted on the left side in the figure.

The same concept for topology optimization can be utilized if two (or more) phases exist, that is, when the void phase is replaced by a second solid material, see structure shown in Figure 2 (b). In this case, the effective linear elastic coefficient $\mathbb{C}$ is written as follows.

$$\mathbb{C} = (1 - s^{\eta})\mathbb{C}_1 + s^{\eta}\mathbb{C}_2, \tag{1}$$

where $\mathbb{C}_1$ and $\mathbb{C}_2$ $(\mathbb{C}_1 \leqslant \mathbb{C}_2)$ are linear elastic coefficients of phase-1 and phase-2, composing solid phases respectively. And s $(0 \leqslant s \leqslant 1)$ indicates a design variable and designates a volume fraction of

DOI: 10.1002/nag

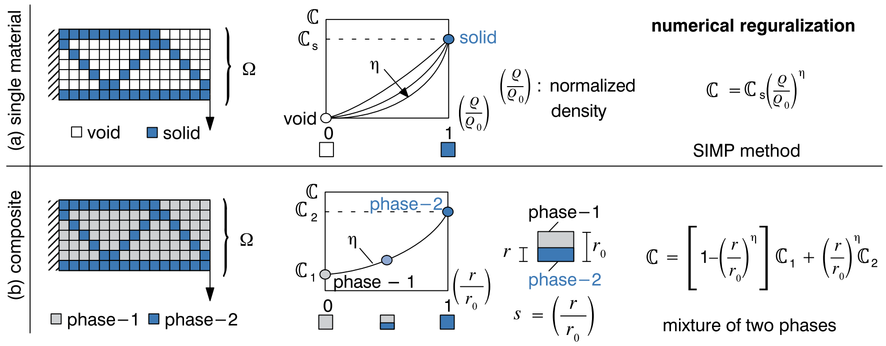

Figure 2. Concept of multiphase material optimization (a) single material topology optimization with SIMP approach and (b) multiphase material optimization (two-phase).

phase-2 in a finite element. As the literature [12] premises the use of a general rectangular element as a finite element, the design variable s is defined as follows;

$$s = r/r_0, \tag{2}$$

where r_0 and r show the height (or width) of a side of a finite element and the actual height (or width) of phase-2 in the element. For instance, if the volume fraction of phase-2 is zero, (i.e., $s = 0$) the entire element is occupied by material of phase-1, and contrarily in the case of $s = 1$, it is occupied by material of phase-2, and in the case of $0 < s < 1$, a mixture of phase-1 and phase-2 appears.

Here, note that as this study employs the embedded reinforcement element introduced in Section 3, the equation for effective linear elastic coefficient slightly differs from Equation (1), which premises the use of general finite elements.

The embedded reinforcement element is a special element superposing stiffness of reinforcement considering position, inclination, and length of reinforcement onto the finite elements of the matrix. That is, we consider by separating the material of natural ground and rockbolts, and artificially apply the concept of two-phase material optimization to the rockbolts. In this case, phase-1 is a non-existent material, and phase-2 is the rockbolts. After substituting $\mathbb{C}_1 = \mathbf{0}$ for the non-existent material and replacing $\mathbb{C}_2$ with the elastic coefficient of the rockbolt $\mathbb{C}^{\mathrm{b}}$ to match an equation to be introduced later, Equation (1) with respect to the uni-axial elastic material coefficient $\mathbb{C}_{\mathrm{L}}^{\mathrm{b}}$ will be arranged as follows because the rockbolts are considered to be one-dimensional.

$$\mathbb{C}_{\mathrm{L}} = s^{\eta}(\mathbb{C}_2)_{\mathrm{L}} = s^{\mathrm{t}}\mathbb{C}_{\mathrm{L}}^{\mathrm{b}}, \tag{3}$$

where $\mathbb{C}_{\mathrm{L}}$ is an effective uni-axial linear elastic material coefficient of the rockbolts and $s^{\mathrm{t}} = r/r_0$ $(0 \leqslant s^{\mathrm{t}} \leqslant 1)$ is a design variable representing thickness of a rockbolt. Meanwhile, r_0, r in the equation are the maximum thickness of the rockbolt in the embedded reinforcement element (known) and the actual thickness respectively, which are to be introduced in Section 3. In this case, based on our artificial assumption of the rockbolt as two-phase material, it is clear that the effective elastic coefficient of the rockbolt is proportionate to the thickness of the rockbolt, and as a result, it is possible to handle it as $\eta = 1$. Then, in the case of $s^{\mathrm{t}} = 0$, the stiffness of the rockbolt becomes zero, which means that no rockbolt is embedded, and in the case of $s^{\mathrm{t}} = 1$, the rockbolt with the maximum thickness r_0 exists in the element. In other words, the present optimization problem turns out to be simply 'thickness optimization' in the embedded reinforcement elements. According to this concept, the optimized thickness of the rockbolt can be determined, and if the thickness is zero, no rockbolt is to be used, that is, the number of rockbolts can be decreased. Figure 3 shows this situation for introducing the design variable s^{t} to the embedded reinforcement.

2.3. Material shape optimization

Discretizing thin linear reinforcement such as rockbolts together with a matrix using general finite elements will create a very complicated element mesh. It is also hard to handle such a finite element mesh

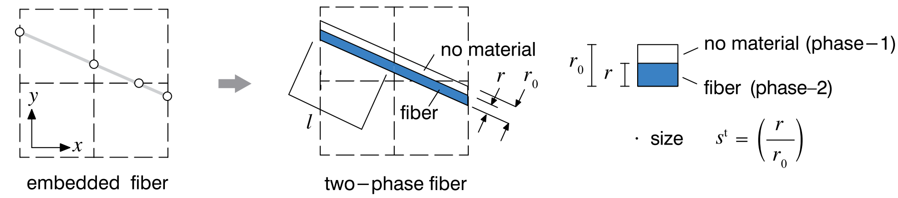

Figure 3. Patches of embedded reinforcement elements.

because it is necessary to regenerate a complicated finite element mesh whenever the layout of the rockbolts is changed in the process of the optimization calculation. So it is common to handle the composite material as homogeneous anisotropic material for simplification and to employ material models on the assumption that the volume fraction of reinforcement material in a finite element and the angles of the fiber reinforcement regarded as the variables for each element [17]. However, as in this type of material model, it is hard to express the exact position of the reinforcement in the elements, and as the reinforcement exhibits discontinuity between adjacent elements, the material model is considered to be mechanically poor in reality.

To solve these problems, material shape optimization, presented in this section, is developed. The material shape optimization is designed to avoid mesh dependency on the elements of the matrix by defining the layout of the reinforcement on the global coordinate system, and as the result, continuous exhibition of reinforcement between elements is made possible. Specifically, global layout of the reinforcement is first parameterized by a function, then the parameterized global layout is embedded into the global structure defined by the global coordinate system, and the layout of the reinforcement is controlled by changing the coordinates of the control point that defines the shape of reinforcement in a parametric space. Incidentally, although the literature [13] studies reinforcement with a curved profile, our study assumes reinforcement with a straight line considering the actual layout of the rockbolts in site. As the result, it is possible to optimize the length, angle, and position of the straight reinforcement by applying this concept.

For reference, a concept diagram of the straight line rockbolts embedded into a structure is shown in Figure 4. Here, when a domain of the entire structure is exhibited in a parametric space as s^{l} $(0 \leqslant s^{\mathrm{l}} \leqslant 1)$, the coordinates of normalized control points, p_0 and p_1, are defined as design variables to determine the actual layout of the rockbolts on the global coordinate system, by which the

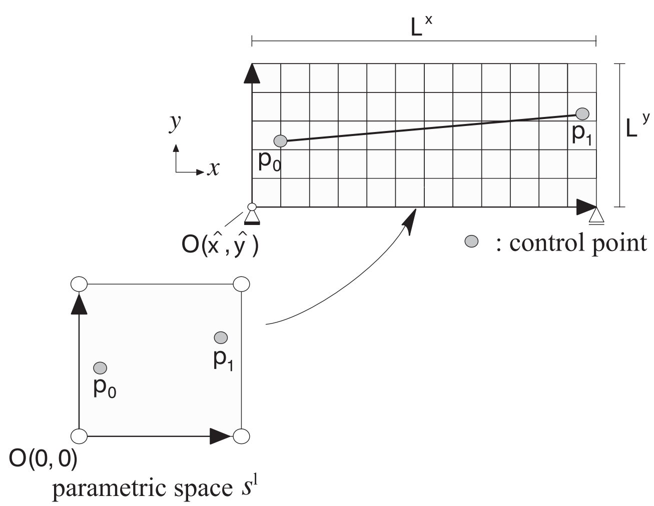

Figure 4. Concept diagram of applying the material shape optimization to a straight-lined reinforcing material.

DOI: 10.1002/nag

lengths of rockbolts can be changed. At this point, the position vector of a jth control point p_j is expressed as follows.

$$\boldsymbol{p}_j\left(s^{\mathrm{l}}_{\mathrm{x},j},\, s^{\mathrm{l}}_{\mathrm{y},j}\right) = \mathrm{O}\left(\hat{x},\, \hat{y}\right) + \left(s^{\mathrm{l}}_{\mathrm{x},j} L^{\mathrm{x}},\, s^{\mathrm{l}}_{\mathrm{y},j} L^{\mathrm{y}}\right), \tag{4}$$

where O indicates the coordinate origin of the structure, and $\hat{x}$ and $\hat{y}$ are the global coordinates corresponding to it. L denotes the outer length of the structure, and the small letters of x and y attached to L and s mean the direction of each. At this point, an arbitrary position vector $\boldsymbol{p}$ of a rockbolt on a global coordinate system is expressed as follows.

$$\boldsymbol{p}(\vartheta,\, \boldsymbol{s}^{\mathrm{l}}) = (1-\vartheta)\,\boldsymbol{p}_1\left(s^{\mathrm{l}}_{\mathrm{x},1},\, s^{\mathrm{l}}_{\mathrm{y},1}\right) + \vartheta\,\boldsymbol{p}_2\left(s^{\mathrm{l}}_{\mathrm{x},2},\, s^{\mathrm{l}}_{\mathrm{y},2}\right), \tag{5}$$

where ϑ $(0 \leqslant \vartheta \leqslant 1)$ shows the local coordinate of the rockbolt.

After determining a global coordinate of a rockbolt, intersection coordinates in the global coordinate system at the rockbolt with the boundary of an element of the natural ground is determined. Then by mapping the intersection coordinates on the natural coordinates of an element, the stiffness matrix of the embedded reinforcement element can be calculated. This mapping procedure is called *nonlinear inverse mapping*. Due to space limitation of this paper, please refer to the literature [13] for the sequence of the process and details thereof.

Multiphase layout optimization is employed to solve the two optimization problems of multiphase material optimization and material shape optimization simultaneously. Please refer to the literatures [1, 2] for details of the process to solve the problem.

3. FINITE ELEMENT FORMULATION CONSIDERING EMBEDDED REINFORCEMENT ELEMENTS

Embedded reinforcement elements have been used for a long period since their development by Phillips and Zienkiewicz [8]. The authors found no examples applying embedded reinforcement elements to rockbolts; however, they are applied to structures or material equipped with straight reinforcement such as fiber-reinforced concrete or underground piles. Balakrishnan and Murray [3] verify the reliability of embedded reinforcement elements by comparing the experimental values of reinforced concrete.

An embedded element consists of reinforcement and a matrix as shown in Figure 5, and stiffness of the reinforcement is to be superposed on stiffness of the matrix. At first, displacement of reinforcement is defined according to that of the matrix as follows.

$$u^{\mathrm{b}}_{\mathrm{L}} = u^{\mathrm{r}}_{\mathrm{L}}, \tag{6}$$

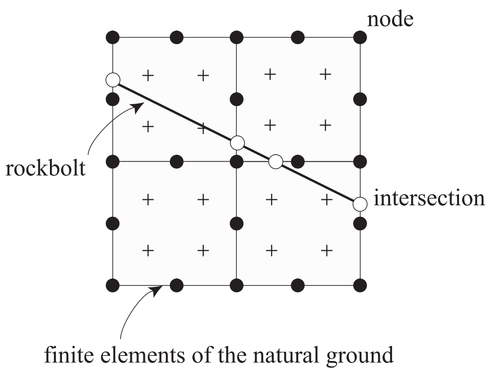

Figure 5. Patches of embedded reinforcement elements.

DOI: 10.1002/nag

where u_L^b and u_L^r stand for displacement fields of a rockbolt and the natural ground, respectively, to the axis direction of the rockbolt at an arbitrary point on the rockbolt. Also, the strain of a rockbolt can be defined as follows.

$$\varepsilon_L^b = \underbrace{\varepsilon_L^r}_{\boldsymbol{T}_1^{\varepsilon}\boldsymbol{\varepsilon}_G^r}, \tag{7}$$

where $\boldsymbol{T}^{\varepsilon}$ is a matrix to transform strain vector $\boldsymbol{\varepsilon}_G$ in a global coordinate system at plane stress condition to the strain vector $\boldsymbol{\varepsilon}_L$ in the local coordinate system. $\boldsymbol{T}_1^{\varepsilon}$ designates the first row of the transformation matrix $\boldsymbol{T}^{\varepsilon}$. In the embedded reinforcement element, reinforcement does not have its own finite element and nodal degrees of freedom. Instead, the displacement and strain in reinforcement is measured by commonly using the nodal displacement vector of the element for the matrix. Therefore, it should be noticed that the layout of the reinforcement does not depend on the mesh. However, as reinforcement is defined as lD model to the axis, the stiffness orthogonal to the axis and the shear stiffness are not considered.

When the virtual work using embedded reinforcement elements is expressed as δW, δW can be divided as follows.

$$\delta W = \delta W_{\text{int}} - \delta W_{\text{ext}} = \delta W_{\text{int}}^{r} + \delta W_{\text{int}}^{b} - \delta W_{\text{ext}} = 0, \tag{8}$$

where $\delta W_{\text{int}}^{r}$ and $\delta W_{\text{int}}^{b}$ represent the virtual work by internal force of the natural ground and rockbolts, respectively, and δW_{ext} denotes the virtual work by external force. Equation (8) is rewritten more specifically as follows.

$$\delta W^{r+b} = \int_{\Omega^{r+b}} \delta\boldsymbol{\varepsilon} : \boldsymbol{\sigma}\, d\Omega^{r+b} - \int_{\Omega^{r+b}} \delta\boldsymbol{u}\cdot\hat{\boldsymbol{b}}\, d\Omega^{r+b} - \int_{\Gamma} \delta\boldsymbol{u}\cdot\hat{\boldsymbol{t}}\, d\Gamma = 0, \tag{9}$$

where $\boldsymbol{\sigma}$ and $\boldsymbol{\varepsilon}$ stand for Cauchy stress tensor and linear strain tensor, respectively. $\hat{\boldsymbol{b}}$ and $\hat{\boldsymbol{t}}$ are the body force vector and the traction force vector, respectively. $\delta\boldsymbol{u}$ indicates the virtual displacement field. Ω and Γ denote the domain of a body and a traction boundary, respectively. Also, it should be noticed that Equation (9) applies to both domains of natural ground and the rockbolts. Further, the internal virtual work of rockbolts in the aforementioned Equation (9) can be simplified by a 1D expression by using the local coordinates system as follows.

$$\delta W_{\text{int}}^{b} = \int_{\Omega^b} \delta\varepsilon_L^b \sigma_L^b\, d\Omega^b = \int_{\Omega^b} \delta\varepsilon_L^r \sigma_L^b\, d\Omega^b. \tag{10}$$

In this study, the displacement field of natural ground is discretized by using the shape function $\boldsymbol{N}$ assuming 8-node rectangular elements,

$$\boldsymbol{u} = \sum_{k=1}^{n_r} N_k d^k \quad \text{or} \quad \boldsymbol{u} = \boldsymbol{N}\boldsymbol{d}. \tag{11}$$

In the aforementioned equation, $\boldsymbol{d}$ is a nodal displacement vector of an element. Also, the local strain of a rockbolt ε_L^b can be rewritten as follows

$$\varepsilon_L^b = \boldsymbol{T}_1^{\varepsilon}\boldsymbol{\varepsilon}_G^r = \boldsymbol{T}_1^{\varepsilon}\boldsymbol{B}^b\boldsymbol{d}. \tag{12}$$

By these equations, the virtual work equation (9) can be discretized as follows

$$\begin{aligned}\delta W &= \delta W_{\text{int}}^{r} + \delta W_{\text{int}}^{b} - \delta W_{\text{ext}} \qquad \forall\, \delta\boldsymbol{d} \\ &= \sum_{e=1}^{n_{\text{ele}}} \delta\boldsymbol{d}^{T} \left[\underbrace{\int_{\Omega^r} \boldsymbol{B}^{r^T}\boldsymbol{\sigma}^r d\Omega^r}_{\boldsymbol{f}_{\text{int}}^{r}} + \underbrace{\int_{\Omega^b} \boldsymbol{B}^{b^T} \left(\boldsymbol{T}_1^{\varepsilon}\right)^T \sigma_L^b\, d\Omega^b}_{\boldsymbol{f}_{\text{int}}^{b}} - \underbrace{\int_{\Gamma} \boldsymbol{N}^T\hat{\boldsymbol{t}}\, d\Gamma}_{\boldsymbol{f}_{\text{ext}}} \right] = 0,\end{aligned} \tag{13}$$

where the body force vector $\hat{\boldsymbol{b}}$ is neglected for simplicity without loss of generality. n_{ele} denotes the number of finite elements. $\boldsymbol{B}^{\mathrm{r}}$ and $\boldsymbol{B}^{\mathrm{b}}$ indicate B-matrix for the natural ground and the rockbolt respectively. As $\boldsymbol{B}^{\mathrm{r}}$ and $\boldsymbol{B}^{\mathrm{b}}$ are the same function, there is no need to distinguish them from each other here. However, the former relates to the integration points of the natural ground and the latter to integration points of the rockbolts. As the difference in this regard will influence future derivation of the sensitivity, they are distinguished here. $\boldsymbol{f}^{\mathrm{r}}_{\mathrm{int}}$ and $\boldsymbol{f}^{\mathrm{b}}_{\mathrm{int}}$ indicate the internal force vector of the natural ground and the rockbolts respectively, and $\boldsymbol{f}_{\mathrm{ext}}$ denotes the external force vector.

Finally, the linear stiffness equation of the finite element method using the embedded reinforcement elements is expressed as follows.

$$\boldsymbol{K}\,\boldsymbol{d} = \boldsymbol{F}, \tag{14}$$

with

$$\begin{aligned}\boldsymbol{K} &= \boldsymbol{K}^{\mathrm{r}} + \boldsymbol{K}^{\mathrm{b}}\\ &= \sum_{\mathrm{e}=1}^{\mathrm{n_{ele}}}\left[\int_{\Omega^{\mathrm{r}}} \boldsymbol{B}^{\mathrm{r}^{\mathrm{T}}}\mathbb{C}^{\mathrm{r}}\boldsymbol{B}^{\mathrm{r}}\mathrm{d}\Omega^{\mathrm{r}} + \int_{\Omega^{\mathrm{b}}} \boldsymbol{B}^{\mathrm{b}^{\mathrm{T}}}\mathbb{C}^{\mathrm{b}}_{\mathrm{G}}\boldsymbol{B}^{\mathrm{b}}\mathrm{d}\Omega^{\mathrm{b}}\right],\end{aligned} \tag{15}$$

$$\boldsymbol{F} = \sum_{\mathrm{e}=1}^{\mathrm{n_{ele}}} \boldsymbol{f}_{\mathrm{ext}}, \tag{16}$$

where $\boldsymbol{K}$ is the global stiffness matrix, $\boldsymbol{K}^{\mathrm{r}}$ and $\boldsymbol{K}^{\mathrm{b}}$ are the stiffness matrices of the natural ground and of rockbolts respectively, and $\boldsymbol{F}$ is the load vector of the global structural system. $\mathbb{C}^{\mathrm{b}}_{\mathrm{G}}$ is an elastic coefficient of the rockbolt expressed for the global coordinate system and is given by the following.

$$\mathbb{C}^{\mathrm{b}}_{\mathrm{G}} = \left(\boldsymbol{T}^{\varepsilon}_{1}\right)^{\mathrm{T}}\mathbb{C}^{\mathrm{b}}_{\mathrm{L}}\boldsymbol{T}^{\varepsilon}_{1}. \tag{17}$$

The effective elastic coefficient to the axis direction of the rockbolts $\mathbb{C}_{\mathrm{L}}$ expressed in Equation (3) does not appear in the aforementioned equation. Actually, to simplify Equation (15), $\mathbb{C}_{\mathrm{L}}$ is divided and a design variable s^{t} in Equation (3) is transferred into $\mathrm{d}\Omega^{\mathrm{b}}$ of Equation (15). So it should be noticed that the stiffness is equivalent to the case using an effective elastic coefficient $\mathbb{C}_{\mathrm{L}}$.

4. ROCKBOLT LAYOUT OPTIMIZATION PROBLEM

4.1. Setting of optimization problem and process to solve

In this section, a rockbolt layout optimization problem with equality constraint is formulated. The objective function thereof is indicated as $f(\boldsymbol{s})$, equality constraint as $h(\boldsymbol{s})$ and the design variable vector as $\boldsymbol{s}$. $\boldsymbol{s}$ indicates a state in which two design variable vectors of thickness and the normalized coordinate at the endpoint of the rockbolts, $\boldsymbol{s}^{\mathrm{t}}$ and $\boldsymbol{s}^{\mathrm{l}}$, are arranged in a row. $\boldsymbol{s}^{\mathrm{t}}$ is assigned to each rockbolt, and the thickness of a rockbolt does not vary along with the axis. Hereafter, design variable is expressed by $\boldsymbol{s}$ for simplification unless specifically needed.

In this study, the stiffness of the entire underground structure including the natural ground and the rockbolts is maximized under a condition that the total volume of the rockbolts used in the whole structure is held constant. Generally, a maximization problem for the stiffness of a structure is handled as mechanically equivalent to the minimization problem for strain energy of the structure. This concept is sketched in Figure 6(a). Although this approach improves the overall stiffness of the whole structure in an average sense under a certain load, it is not intended to maximize stiffness for lessening deformation at a specific location. However, in the case of tunnel digging, far larger deformation exceeding prior assumptions may happen occasionally on the tunnel ceiling or side walls. For such cases, layout of rockbolts to restrain the deformation at a minimum level must be determined with urgent priority. In such cases, the most significant deformation location is to be determined as the displacement-controlled point on the structural analysis and finding out a layout of rockbolts to ‘maximize’ the strain energy can maximize the stiffness of the entire structure, see the sketch shown in Figure 6(b).

DOI: 10.1002/nag

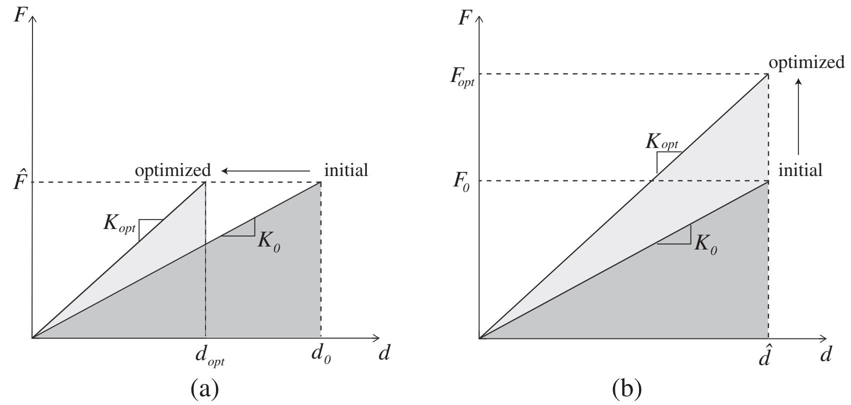

Figure 6. Strategy for maximization of stiffness. (a) minimizing strain energy under constant load level and (b) maximizing strain energy with keeping displacement at displacement-controlled point constant.

In consideration of the aforementioned text, this study employs an approach to maximize the strain energy with respect to the corresponding component of displacement vector at the displacement-controlled point, that is, the latter approach. The optimization problem of this study is described as follows.

$$\text{minimize} \quad f(\boldsymbol{s}) = -\int_{\Omega^{\mathrm{r+b}}} \boldsymbol{\varepsilon}^{\mathrm{T}} \boldsymbol{\sigma} \, \mathrm{d}\Omega^{\mathrm{r+b}}, \tag{18}$$

$$\text{subject to} \quad h(\boldsymbol{s}) = \sum_{m=1}^{n_{\mathrm{ele}}^{\mathrm{b}}} \int_{\Omega_{\xi}^{\mathrm{b}}} \underbrace{|\boldsymbol{J}^{\mathrm{b}}|}_{s^{\mathrm{t}} r_0 l} \, \mathrm{d}\Omega_{\xi}^{\mathrm{b}} - \hat{V} = 0, \tag{19}$$

$$\boldsymbol{s}_{\mathrm{L}}^{\mathrm{t}} \leqslant \boldsymbol{s}_i^{\mathrm{t}} \leqslant \boldsymbol{s}_{\mathrm{U}}^{\mathrm{t}} \quad i = 1, \ldots, n_{\mathrm{s}}^{\mathrm{t}}, \tag{20}$$

$$\boldsymbol{s}_{\mathrm{L}}^{\mathrm{l}} \leqslant \boldsymbol{s}_i^{\mathrm{l}} \leqslant \boldsymbol{s}_{\mathrm{U}}^{\mathrm{l}} \quad i = 1, \ldots, n_{\mathrm{s}}^{\mathrm{l}}, \tag{21}$$

where ξ means natural coordinate space and $|\boldsymbol{J}^{\mathrm{b}}|$ expresses the determinant of Jacobian matrix of rockbolts. r_0 signifies the maximum thickness of the rockbolts as mentioned earlier and fixed as constant to the length direction. l indicates the length of a rockbolt in the embedded element as shown in Figure 3 and depends on design variable of s^{l}. $\hat{V}$ denotes the prescribed total volume of rockbolts in the entire structure, $\boldsymbol{s}_{\mathrm{L}}$ and $\boldsymbol{s}_{\mathrm{U}}$ are the lower and upper bounds of design variables, and n_{s} indicates the number of design variables. Superscripts t and l on $\boldsymbol{s}$ and n_{s} mean the terms related to the design variable s^{t} and s^{l}, respectively. $n_{\mathrm{ele}}^{\mathrm{b}}$ is the total number of elements for the natural ground having rockbolts, and varies according to changes of length and position of rockbolts during optimization. Further, as the optimization problem is set to minimize the objective function, we converted the strain energy to a negative number in Equation (18). Here, for reference, the optimization process is illustrated in Figure 7. As this study applies a gradient-based optimization algorithm, the sensitivity with respect to design variables of the objective function and constraint, $\nabla_s f$ and $\nabla_s h$, must be gained. The sensitivity thus obtained is incorporated into the optimization algorithm to produce the optimization solution at that point, and then the calculation is to be continued until converged. In the following section, a method to derive the sensitivities of the objective and constraint functions is described.

4.2. Calculation of sensitivity coefficients

4.2.1. Sensitivity of objective function. The objective function in this study f depends on not only design variable $\boldsymbol{s}$ but also displacement $\boldsymbol{d}$, and further, the displacement $\boldsymbol{d}$ depends on design variable

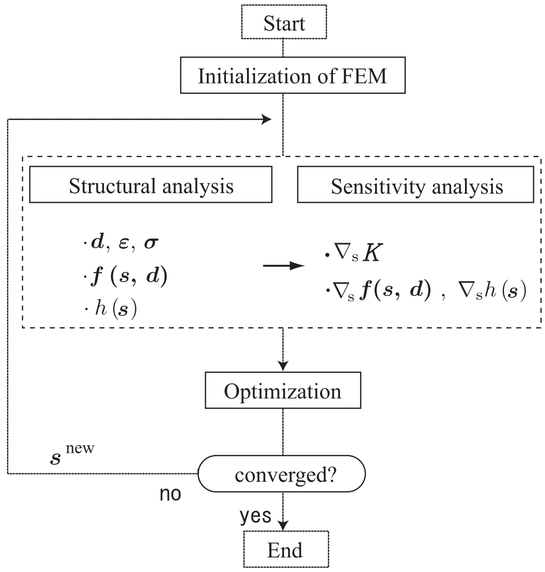

Figure 7. Process to solve the optimization problem.

$\boldsymbol{s}$. From this, the total derivative of objective function, $f = f(\boldsymbol{s}, \boldsymbol{d})$, with respect to design variable $\boldsymbol{s}$ is shown as follows by the chain rule,

$$\begin{aligned}\nabla_s f(\boldsymbol{s}, \boldsymbol{d}) &= \frac{\partial f}{\partial s} + \frac{\partial f}{\partial \boldsymbol{d}} \frac{\partial \boldsymbol{d}}{\partial s}, \\ &= \nabla_s^{\text{ex}} f + \nabla_d f^{\mathrm{T}} \nabla_s \boldsymbol{d},\end{aligned} \tag{22}$$

where $\nabla_s^{\text{ex}}(\bullet)$ means a differential term gained explicitly. As the nodal displacement vector $\boldsymbol{d}$ is an unknown factor in the structural analysis, the differentiation with respect to design variables, $\nabla_s \boldsymbol{d}$, cannot be directly obtained. Thus, the virtual work equation (13) is differentiated with respect to the design variable $\boldsymbol{s}$ to derive $\nabla_s \boldsymbol{d}$ indirectly. As the optimization problem in this study is a comparatively simple linear problem, the term of $\nabla_s \boldsymbol{d}$ is deleted by applying the related equation, and finally, the following simple sensitivity equation is derived.

$$\nabla_s f = -\boldsymbol{d}^{\mathrm{T}} \nabla_s \boldsymbol{K} \boldsymbol{d}. \tag{23}$$

As shown in this equation, the differential term is only a $\nabla_s \boldsymbol{K}$, which is gained explicitly, and thus, the sensitivity of the objective function can be calculated easily. The process to achieve Equation (23) is described in detail in Appendix.

4.2.2. Sensitivity of equality constraint. As the equation of the equality constraint condition (19) does not depend on displacement $\boldsymbol{d}$, the derivative of the equality constraint with respect to the design variable $\boldsymbol{s}$ is shown as follows.

$$\nabla_s h = \frac{\mathrm{d}h(\boldsymbol{s})}{\mathrm{d}s}. \tag{24}$$

As this is obtained explicitly, the sensitivity of the equality constraint is written as the following equation,

$$\nabla_s h = \sum_{m=1}^{n_{\text{ele}}^{\text{b}}} \int_{\Omega_\xi^{\text{b}}} (\nabla_s |\boldsymbol{J}^{\text{b}}|) \, \mathrm{d}\Omega_\xi^{\text{b}}. \tag{25}$$

DOI: 10.1002/nag

5. EXAMPLES OF OPTIMIZATION CALCULATION

In this section, applicability of the proposed optimization method for the layout of rockbolts is verified with two numerical examples: one for rockbolts for tunnel support of NATM, and the other for reinforcing side slopes.

5.1. *Optimization of layout of rockbolts for NATM*

5.1.1. Conditions of analysis. Figure 8 illustrates the assumed ground structure model. In this example, a cross-section of a round-face tunnel excavation is adopted for simplicity. Embedded reinforcement element based on 8-node quadrilateral element is applied and the total number of the element is 864. All the materials are assumed to be linearly elastic, and the material properties are shown in Table I.

Layout of rockbolts before optimization is set in accordance with the standard support pattern; the length of all rockbolts is set to be 8000 mm, and the thickness is 25 mm. Although the actual record for the downward rockbolts is quite limited, we allow to use such a layout of rockbolts to observe the structural response. The lower bound of the thickness of the rockbolt is set to 0 mm, and the upper bound to 50 mm. As a result, the initial value of the design valuable $\boldsymbol{s}^{\mathrm{t}}$ comes out to be 0.5. After the tunnel-side tip of a rockbolt on the surface of the tunnel excavation is fixed, the length of the rockbolts is altered by moving the other tip toward the axis direction of the rockbolt. Of course, it is possible to move the coordinate of the end tip two-dimensionally. However, in such a case, some rockbolts may cross each other because of the change of angles of rockbolts during optimization. To prevent such a

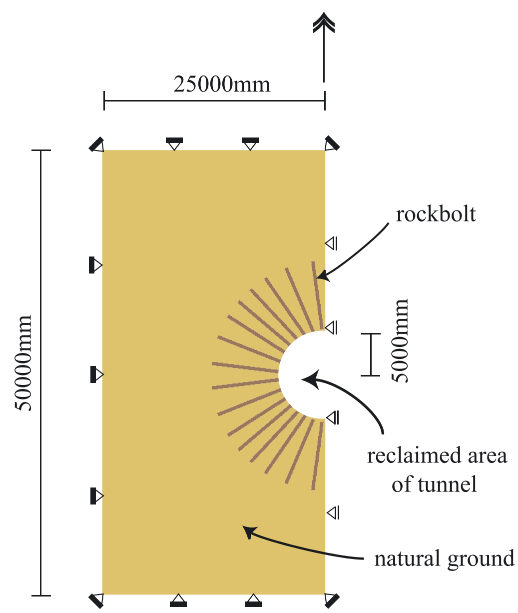

Figure 8. Ground structure model.

Table I. NATM: material properties.

	Young's modulus (N/mm^2)	Poisson's ratio
Rockbolt	240,000	0.2
Natural ground	50,000	0.25

DOI: 10.1002/nag

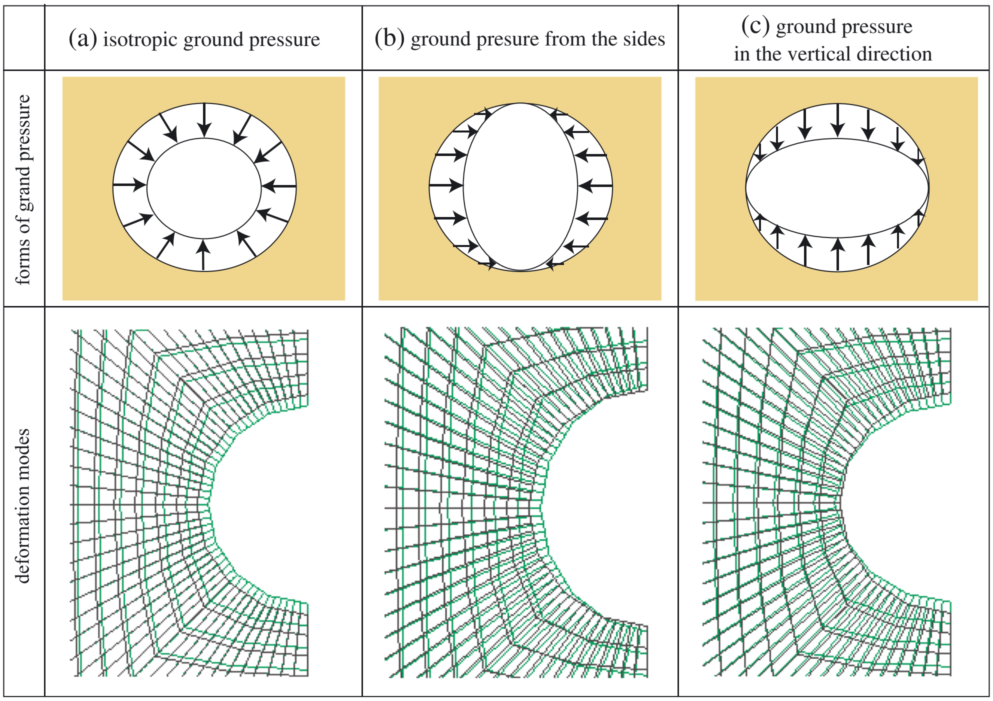

Figure 9. Forms of assumed ground pressure (upper figures), undeformed meshes (black), and deformation modes (green) of unreinforced natural ground: (a) case when the structure is subject to isotropic ground pressure, (b) case when ground pressure from the sides dominates, and (c) case when ground pressure in the vertical direction dominates.

situation, the initial angle of each rockbolt is set to be unchanged. The coordinate origin O in the parametric space of $\boldsymbol{s}^1$ is set on the corner at the bottom left of Figure 8. And, as explained in the equality constraint, the total volume of the rockbolts remains unchanged during the optimization.

In this example of the NATM, we assume for simplicity that the ground pressure is to be released after excavating the tunnel. Here, three cases of optimization under different loading conditions as illustrated in Figure 9 are demonstrated: (a) subject to isotropic ground pressure, (b) the ground pressure from sides dominate, and (c) the ground pressure to the vertical direction dominates. For the case of Figure 9(a), the surface load is provided as a uniformly distributed load (10 N/mm), and for the other cases, that is Figure 9(b, c), the maximum value of distributed load from horizontal or vertical slanted shadow is set to 10 N/mm. The displacement-controlled node is set to the location where the maximum displacement is observed in each loading condition. The following are the results of optimization for the three different load cases.

5.1.2. Case: subjected to isotropic ground pressure. Figure 10 illustrates the optimization results of the case that is subjected to isotropic ground pressure. The left side of Figure 10 shows the layout of rockbolts after optimization, and the right side shows the uni-axial stress of the rockbolts. In this calculation, we tried to maximize the stiffness of the entire structure for a prescribed displacement to the vertical downward direction at the ceiling of the excavated surface $(x, y) = (25,000, 30,000)$, that is, the displacement-controlled node. Of course, other nodes on the excavated surface may be chosen as the controlled point because isotropic pressure is subjected. Figure 9(a) at the bottom shows the deformation mode of unreinforced natural ground. As can be seen from these two diagrams, uniformly high stress occurs around the excavating area, and thick and short rockbolts are laid out radially to the center of the tunnel to reinforce the stressed area. Thickness of the rockbolts reaches a maximum of 50 mm. Here, some differences in the length of the rockbolts are seen, but it is understood as the influence of rectangular design domain. The results obtained show a layout similar to the standard support

DOI: 10.1002/nag

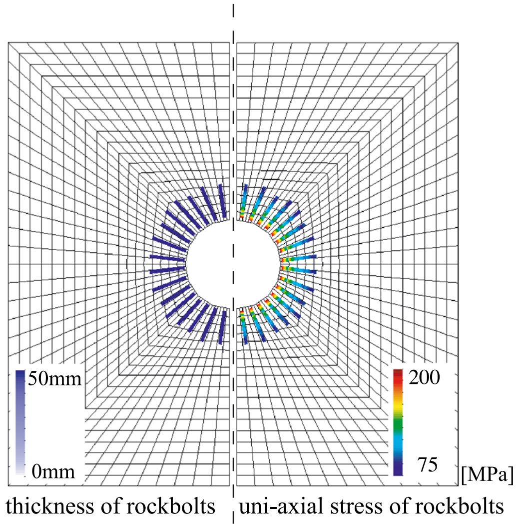

Figure 10. Optimization results subjected to isotropic ground pressure.

pattern. Thus, it was verified that the standard support pattern is effective with respect to the isotropic ground pressure.

5.1.3. Case: ground pressure from side dominates. In case the tunnel is subjected to high ground pressure from both sides, the tunnel shows a deformation mode to narrow the width as shown in Figure 9(b) bottom. So, we set a displacement-controlled point at the center node of the left side of the tunnel excavating area, $(x, y) = (20,000, 25,000)$, and the controlled degree of freedom is taken to the horizontal right direction (plus x direction). Figure 11 shows the result of the optimization. Also, Figure 12 shows the history of the value of the objective function, in which the function value is decreased rapidly soon after the optimization calculation, and according to the increase of the number of optimization steps, it is noticed that the value converged into a certain value. The total optimization step number is 70.

As Figure 11 shows, almost all materials for rockbolts are employed to reinforcement of side directions. The upward and downward rockbolts vanished with zero thickness expect for the top and bottom

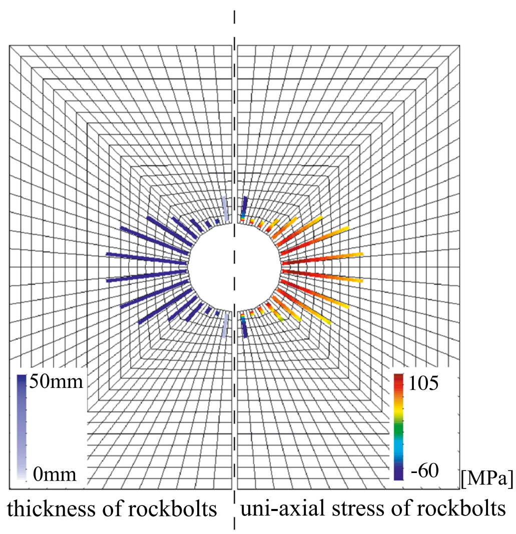

Figure 11. Optimization results where the ground pressure from sides dominates.

DOI: 10.1002/nag

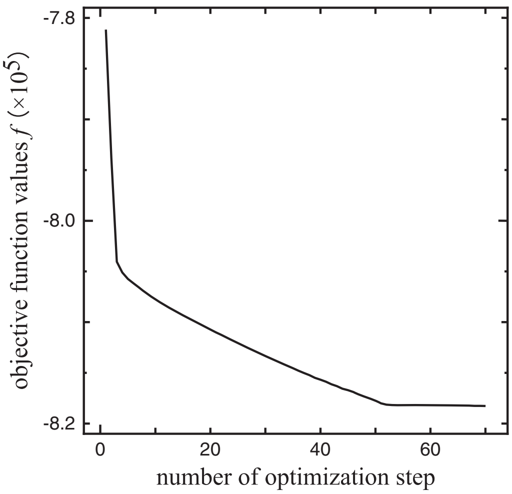

Figure 12. History of objective function value.

short ones that reinforce the top and bottom part of the cross-section where the vertical compressive stresses dominate.

This optimization result is reasonable and it was verified that the present optimization method provides optimal layout of rockbolts. However, in design, we expect rockbolts to act as reinforcement against tension but compression. Thus, in the actual construction, the top/bottom short rockbolts for compression may be removed. This results from that our objective function is based on strain energy in which no distinction is paid between tension and compression.

5.1.4. Case: the ground pressure in the vertical direction dominates. In case the tunnel is subjected to high ground pressure in the vertical direction, the tunnel shows a deformation mode to lessen the height of the tunnel inside as shown in Figure 9(c) at bottom. The displacement-controlled point is set at the ceiling of the tunnel excavation $(x, y) = (25,000, 30,000)$, and its controlled degree of freedom is set to the minus y-direction.

Figure 13 shows the result of optimization, which is similar to that of the previous section except for the direction of the ground pressure and does not indicate any new particular findings. However, the

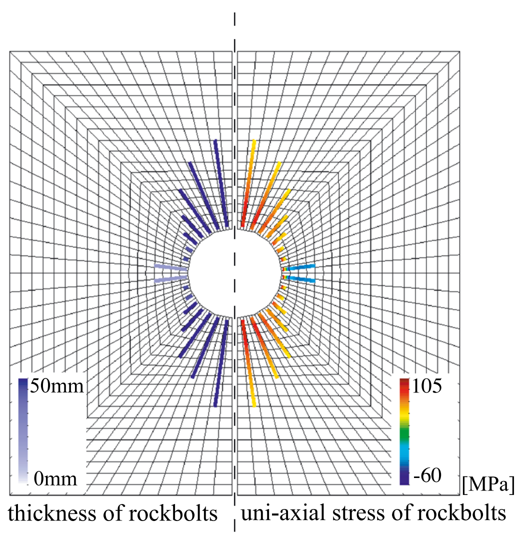

Figure 13. Optimization results where the vertical ground pressure dominates.

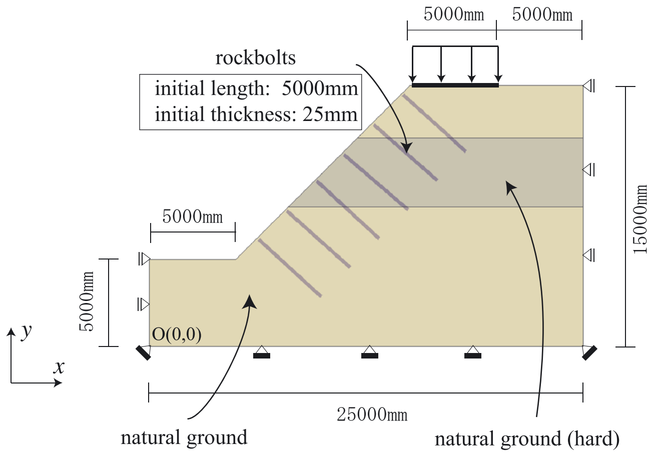

Figure 14. Structural model for reinforcing slopes.

Table II. Reinforcing slopes: material properties.

	Young's modulus (N/mm^2)	Poisson's ratio
Rockbolt	240,000	0.2
Natural ground	50,000	0.25
Natural ground (hard)	75,000	0.25

reliability of this method is verified in the sense that a series of algorithms for multiphase layout optimization can steadily provide a similar optimization solution, even when the direction of the natural ground pressure is altered. As the changes of the value of objective function shows similar tendency to the previous one, it is eliminated here.

From the aforementioned text, the rockbolt layout optimization method based on the multiphase layout optimization is verified to provide the most reasonable layout for tunnels under the anisotropic natural ground pressure.

5.2. *Rockbolt layout optimization for reinforcing slopes*

As the second numerical example, the layout of rockbolts is optimized for a reinforced slope. Figure 14 is a structural model of the reinforced slope used for this example. Here, a stratum consisting of three horizontal layers by inserting a comparatively hard layer in the midst is assumed. A uniformly distributed vertical load of 1 kN/mm is applied, and six rockbolts are installed perpendicularly to the slope. In this design problem, we assume that the displacement at the top corner of the slope should be reduced by optimization. Thus, minus x-direction at the top corner of the slope is simply chosen as the degree of freedom of the displacement controlled node. Embedded reinforcement element based on 8-node quadrilateral element is applied, and the total number of elements is 410. Linearly elastic materials are employed similarly to the previous examples, and the material properties are shown in Table II. The initial values of length and thickness of the rockbolts are set as 5000 mm and 25 mm, respectively. The lower bound of thickness of the rockbolts is set to 0 mm and the upper bound to 50 mm. The tip of the rockbolt is fixed on the slope, and moving the other tip to the axis direction alters the length of rockbolts. For reference, Figure 15 displays the distribution of shear stress of the natural ground before reinforcing, and Figure 16 shows the distribution of uni-axial stress in rockbolts before optimization.

In this section, two different cases with respect to the maximum length of rockbolts are applied. The first case is that no limitation on the maximum length of rockbolts within the design space is placed. Incidentally, in the following examples, length of rockbolts is introduced as the result of optimization

DOI: 10.1002/nag

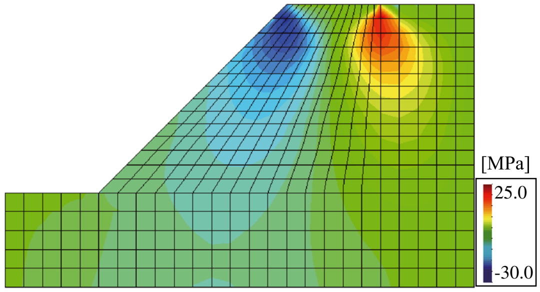

Figure 15. Distribution of shear stress of unreinforced natural ground.

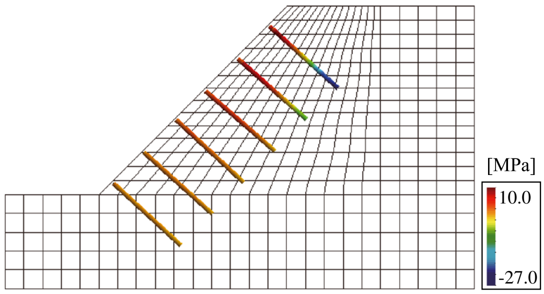

Figure 16. Uni-axial stress of rockbolts before optimization.

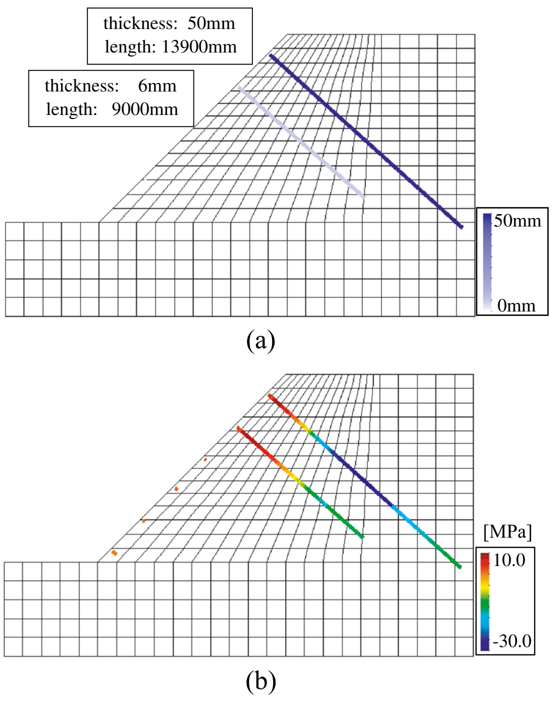

Figure 17. Optimization results without limitation for maximum length of rockbolts. (a) optimized layout and (b) uni-axial stress of rockbolts.

instead of listing the optimal coordinates of the endpoints of rockbolts $\boldsymbol{s}^1$ because it is easy for readers to understand the optimal layout of rockbolts.

Figure 17(a) and (b) shows the optimized layout of rockbolts and its uni-axial stress distribution for the former case, respectively. The total number of optimization step is 196. In this case, most material

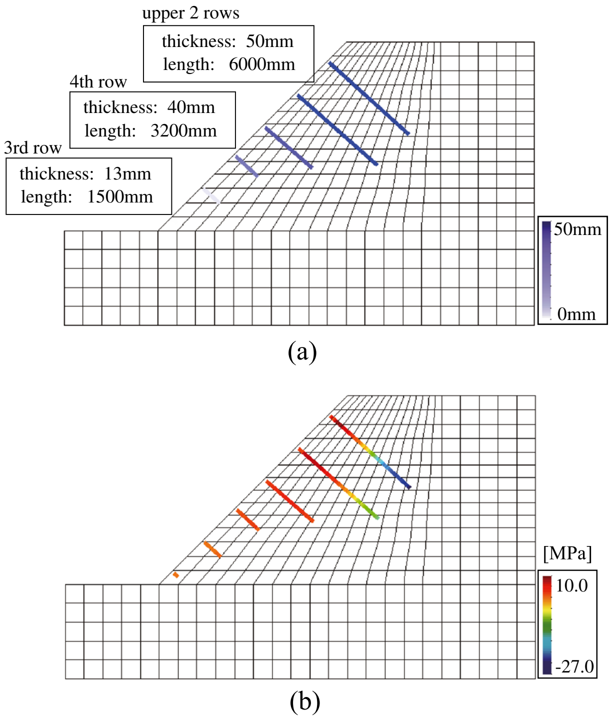

Figure 18. Optimization results with limitation for maximum length of rockbolts (6000 mm). (a) optimized layout and (b) uni-axial stress of rockbolts.

for rockbolt assembled at the sixth row (top row) and the thickness of the row reached the maximum of 50 mm with almost 14 m of length. However, this rockbolt reinforces the most severe location, where the compressive stress in the rockbolt reaches 30 MPa. The sixth row rockbolt plays a significant role in preventing the possible circular slip of natural ground for slope stability. The fifth row also plays a role in reinforcing the slope by fixing to the hard stratum. For this reason, the obtained layout of rockbolts should be structurally reasonable. However, length of 14 m of rockbolt is too long from a viewpoint of the actual design in geotechnical engineering.

The second one is that the maximum length of the rockbolts is set to 6000 mm in considering the actual construction work. Figure 18(a) and (b) shows the optimized layout of rockbolts and its uni-axial stress distribution, respectively. The total number of optimization step is 83. In this case, the thickness of the upper two rows of rockbolts reached the maximum of 50 mm, and the length reached the upper limit, so as to reinforce against the stress concentration. Also, the length of the rockbolts on the third and fourth rows is changed in accordance with the magnitude of stresses. This layout of rockbolts reinforces the entire slope in average sense. On the other hand, the thicknesses of the two lower rockbolts become almost zero; this reduces the number of rockbolts.

From these results, it was shown that the method for multiphase layout optimization can successfully apply for reinforcing slopes by rockbolts in the sense that the optimized layout provides a mechanically reasonable from a viewpoint of the actual design.

To summarize, multiphase layout optimization is a very effective method for reinforcement design because changing only two design variables, that is length and thicknesses of reinforcement, can control the number and location of reinforcement indirectly.

6. CONCLUSIONS

The aims of this study are as follows: (i) to develop a method for maximizing the stiffness of the entire structure of the natural ground by applying the multiphase layout optimization to the rockbolt support

DOI: 10.1002/nag

systems, which are used in the NATM and reinforcing slopes; and (ii) to verify the applicability of this method by confirming the differences with the traditionally used standard rockbolt-support pattern.

Results of our study are described hereunder.

- The study formulates a method to maximize the stiffness of a structure by maximizing the strain energy for a prescribed displacement at the specified controlled point, contrary to the traditional method to minimize the strain energy. By this method, even if unexpected deformation exceeding the prior assumption in the excavating site of the tunnels is confirmed, the optimized rockbolt layout to restrain the deformation can be determined with the top priority.
- In the numerical examples, mechanically reasonable optimized structures were obtained in each case. Also, in the case of providing an upper bound of the length of the rockbolts due to construction work, satisfactory results are gained similarly. Including the aforementioned results, the method is verified to have enough feasibility for application to actual design.

Subject for further research is considered to be as follows.

- It is necessary to extend the method of optimization to consider nonlinear material properties for more actual rockbolt layout, because the materials of natural ground actually exhibit very complicated behavior.
- Although the rockbolts are fundamentally used as tension members, in case of the objective function based on the strain energy, compression and tensile strength are treated equally without distinction. In this connection, it is considered that if we can formulate an optimization problem to exclude the influence of compression stress of the rockbolts, it will produce a more effective rockbolt layout.
- Although 2D models were demonstrated in the present paper, the extension to 3D model is essential to achieve a more realistic design for natural ground reinforcement.

APPENDIX A: SENSITIVITY OF OBJECTIVE FUNCTION

Here, the sensitivity of the objective function $\nabla_{\boldsymbol{s}} f$ with respect to the design variable $\boldsymbol{s}$ shown in Equation (23) is derived. To avoid the complexity of the equation, the design variable $\boldsymbol{s} = \{\boldsymbol{s}^{\mathrm{t}} \cup \boldsymbol{s}^{\mathrm{l}}\}$, and $\boldsymbol{T} \equiv \boldsymbol{T}^{\varepsilon}$ are used here. First, by using the stress–strain relation, we rewrite Equation (18) as follows.

$$f(\boldsymbol{s}) = -\int\limits_{\Omega^{\mathrm{r+b}}} \boldsymbol{\varepsilon}^{\mathrm{T}} \mathbb{C}_{\mathrm{G}} \boldsymbol{\varepsilon} \mathrm{d}\Omega^{\mathrm{r+b}}, \tag{26}$$

where $\mathbb{C}_{\mathrm{G}}$ is a linear material stiffness matrix in the global coordinate system. Equation (26) is rewritten, dividing by each material as follows;

$$f(\boldsymbol{s}) = -\int\limits_{\Omega^{\mathrm{b}}} \boldsymbol{\varepsilon}^{\mathrm{b}^{\mathrm{T}}} \mathbb{C}_{\mathrm{G}}^{\mathrm{b}} \boldsymbol{\varepsilon}^{\mathrm{b}} \mathrm{d}\Omega^{\mathrm{b}} - \int\limits_{\Omega^{\mathrm{r}}} \boldsymbol{\varepsilon}^{\mathrm{r}^{\mathrm{T}}} \mathbb{C}^{\mathrm{r}} \boldsymbol{\varepsilon}^{\mathrm{r}} \mathrm{d}\Omega^{\mathrm{r}}. \tag{27}$$

$\mathbb{C}_{\mathrm{G}}^{\mathrm{b}}$ is the material stiffness matrix of rockbolts in the global coordinate system. Then, after the first term of Equation (27) is extracted and differentiated by design variable $\boldsymbol{s}$, the following equation is obtained,

$$\begin{aligned}\nabla_{s}\left(\int\limits_{\Omega^{\mathrm{b}}} \boldsymbol{\varepsilon}^{\mathrm{b}^{\mathrm{T}}} \mathbb{C}_{\mathrm{G}}^{\mathrm{b}} \boldsymbol{\varepsilon}^{\mathrm{b}} \mathrm{d}\Omega^{\mathrm{b}}\right) &= \int\limits_{\Omega^{\mathrm{b}}} (\nabla_{s} \boldsymbol{\varepsilon}^{\mathrm{b}^{\mathrm{T}}}) \mathbb{C}_{\mathrm{G}}^{\mathrm{b}} \boldsymbol{\varepsilon}^{\mathrm{b}} \mathrm{d}\Omega^{\mathrm{b}} + \int\limits_{\Omega^{\mathrm{b}}} \boldsymbol{\varepsilon}^{\mathrm{b}^{\mathrm{T}}} \left(\nabla_{s} \mathbb{C}_{\mathrm{G}}^{\mathrm{b}}\right) \boldsymbol{\varepsilon}^{\mathrm{b}} \mathrm{d}\Omega^{\mathrm{b}} \\ &+ \int\limits_{\Omega^{\mathrm{b}}} \boldsymbol{\varepsilon}^{\mathrm{b}^{\mathrm{T}}} \mathbb{C}_{\mathrm{G}}^{\mathrm{b}} (\nabla_{s} \boldsymbol{\varepsilon}^{\mathrm{b}}) \mathrm{d}\Omega^{\mathrm{b}} + \int\limits_{\Omega^{\mathrm{b}}} \boldsymbol{\varepsilon}^{\mathrm{b}^{\mathrm{T}}} \mathbb{C}_{\mathrm{G}}^{\mathrm{b}} \boldsymbol{\varepsilon}^{\mathrm{b}} (\nabla_{s} \mathrm{d}\Omega^{\mathrm{b}}).\end{aligned} \tag{28}$$

DOI: 10.1002/nag

Here, by using the relation of $\boldsymbol{\varepsilon}^{\mathrm{b}} = \boldsymbol{B}^{\mathrm{b}}\boldsymbol{d}$, we arrange Equation (28) as follows.

$$\begin{aligned}\nabla_s\left(\int_{\Omega^{\mathrm{b}}} \boldsymbol{\varepsilon}^{\mathrm{b}^{\mathrm{T}}}\mathbb{C}^{\mathrm{b}}_{\mathrm{G}}\boldsymbol{\varepsilon}^{\mathrm{b}}\mathrm{d}\Omega^{\mathrm{b}}\right) &= \int_{\Omega^{\mathrm{b}}} \boldsymbol{d}^{\mathrm{T}}(\nabla_s\boldsymbol{B}^{\mathrm{b}^{\mathrm{T}}})\mathbb{C}^{\mathrm{b}}_{\mathrm{G}}\boldsymbol{B}^{\mathrm{b}}\boldsymbol{d}\,\mathrm{d}\Omega^{\mathrm{b}} + \int_{\Omega^{\mathrm{b}}} \boldsymbol{d}^{\mathrm{T}}\boldsymbol{B}^{\mathrm{b}^{\mathrm{T}}}\left(\nabla_s\mathbb{C}^{\mathrm{b}}_{\mathrm{G}}\right)\boldsymbol{B}^{\mathrm{b}}\boldsymbol{d}\,\mathrm{d}\Omega^{\mathrm{b}} \\ &\quad + \int_{\Omega^{\mathrm{b}}} \boldsymbol{d}^{\mathrm{T}}\boldsymbol{B}^{\mathrm{b}^{\mathrm{T}}}\mathbb{C}^{\mathrm{b}}_{\mathrm{G}}(\nabla_s\boldsymbol{B}^{\mathrm{b}})\boldsymbol{d}\,\mathrm{d}\Omega^{\mathrm{b}} + 2\int_{\Omega^{\mathrm{b}}} \boldsymbol{d}^{\mathrm{T}}\boldsymbol{B}^{\mathrm{b}^{\mathrm{T}}}\mathbb{C}^{\mathrm{b}}_{\mathrm{G}}\boldsymbol{B}^{\mathrm{b}}(\nabla_s\boldsymbol{d})\mathrm{d}\Omega^{\mathrm{b}} \\ &\quad + \int_{\Omega^{\mathrm{b}}} \boldsymbol{d}^{\mathrm{T}}\boldsymbol{B}^{\mathrm{b}^{\mathrm{T}}}\mathbb{C}^{\mathrm{b}}_{\mathrm{G}}\boldsymbol{B}^{\mathrm{b}}\boldsymbol{d}\,(\nabla_s\mathrm{d}\Omega^{\mathrm{b}}).\end{aligned} \tag{29}$$

Then, the 2nd term of Equation (27) is differentiated by design variable $\boldsymbol{s}$. In this calculation, as the following function and terms for natural ground, $\boldsymbol{B}^{\mathrm{r}}$, $\mathbb{C}^{\mathrm{r}}$, and $\mathrm{d}\Omega^{\mathrm{r}}$, do not depend on the design variable $\boldsymbol{s}$; their differential terms become zero; thus, the equation can be simplified as follows.

$$\nabla_s\left(\int_{\Omega^{\mathrm{r}}} \boldsymbol{\varepsilon}^{\mathrm{r}^{\mathrm{T}}}\mathbb{C}^{\mathrm{r}}\boldsymbol{\varepsilon}^{\mathrm{r}}\mathrm{d}\Omega^{\mathrm{r}}\right) = 2\int_{\Omega^{\mathrm{r}}} \boldsymbol{d}^{\mathrm{T}}\boldsymbol{B}^{\mathrm{r}^{\mathrm{T}}}\mathbb{C}^{\mathrm{r}}_{\mathrm{G}}\boldsymbol{B}^{\mathrm{r}}(\nabla_s\boldsymbol{d})\mathrm{d}\Omega^{\mathrm{r}}. \tag{30}$$

However, $\nabla_s\boldsymbol{d}$ in Equations (29) and (30) is not obtained explicitly. Therefore, by using the virtual work Equation (13), we derive $\nabla_s\boldsymbol{d}$ indirectly.

First, the whole Equation (13) is differentiated with respect to design variable $\boldsymbol{s}$. In this study, the traction force vector, $\hat{\boldsymbol{t}}$, is assumed to be independent of design variable $\boldsymbol{s}$, and the virtual displacement, $\delta\boldsymbol{d}$, does not depend on $\boldsymbol{s}$ because of its arbitrariness. Based on this assumption, Equation (13) is differentiated with respect to the design variable $\boldsymbol{s}$ as follows.

$$\nabla_s\left(\int_{\Omega^{\mathrm{b}}} \boldsymbol{B}^{\mathrm{r}^{\mathrm{T}}}\mathbb{C}^{\mathrm{b}}_{\mathrm{G}}\boldsymbol{B}^{\mathrm{r}}\boldsymbol{d}\,\mathrm{d}\Omega^{\mathrm{b}} + \int_{\Omega^{\mathrm{r}}} \boldsymbol{B}^{\mathrm{r}^{\mathrm{T}}}\mathbb{C}^{\mathrm{r}}_{\mathrm{G}}\boldsymbol{B}^{\mathrm{r}}\boldsymbol{d}\,\mathrm{d}\Omega^{\mathrm{r}}\right) = 0. \tag{31}$$

The aforementioned equation is expanded in turn and arranged by transferring the terms including $\nabla_s\boldsymbol{d}$ to the left-hand side and the others to the right-hand side of the equation as follows.

$$\begin{aligned}\int_{\Omega^{\mathrm{b}}}\boldsymbol{B}^{\mathrm{b}^{\mathrm{T}}}\mathbb{C}^{\mathrm{b}}_{\mathrm{G}}\boldsymbol{B}^{\mathrm{b}}\mathrm{d}\Omega^{\mathrm{b}}(\nabla_s\boldsymbol{d}) + \int_{\Omega^{\mathrm{r}}} \boldsymbol{B}^{\mathrm{r}^{\mathrm{T}}}\mathbb{C}^{\mathrm{b}}_{\mathrm{G}}\boldsymbol{B}^{\mathrm{r}}\mathrm{d}\Omega^{\mathrm{r}}(\nabla_s\boldsymbol{d}) &= -\int_{\Omega^{\mathrm{b}}}(\nabla_s\boldsymbol{B}^{\mathrm{b}^{\mathrm{T}}})\mathbb{C}^{\mathrm{b}}_{\mathrm{G}}\boldsymbol{B}^{\mathrm{b}}\boldsymbol{d}\,\mathrm{d}\Omega^{\mathrm{b}} - \int_{\Omega^{\mathrm{b}}} \boldsymbol{B}^{\mathrm{b}^{\mathrm{T}}}\left(\nabla_s\mathbb{C}^{\mathrm{b}}_{\mathrm{G}}\right)\boldsymbol{B}^{\mathrm{b}}\boldsymbol{d}\,\mathrm{d}\Omega^{\mathrm{b}} \\ &\quad - \int_{\Omega^{\mathrm{b}}} \boldsymbol{B}^{\mathrm{b}^{\mathrm{T}}}\mathbb{C}^{\mathrm{b}}_{\mathrm{G}}(\nabla_s\boldsymbol{B}^{\mathrm{b}})\boldsymbol{d}\,\mathrm{d}\Omega^{\mathrm{b}} - \int_{\Omega^{\mathrm{b}}} \boldsymbol{B}^{\mathrm{b}^{\mathrm{T}}}\mathbb{C}^{\mathrm{b}}_{\mathrm{G}}\boldsymbol{B}^{\mathrm{b}}\boldsymbol{d}\,(\nabla_s\mathrm{d}\Omega^{\mathrm{b}}).\end{aligned} \tag{32}$$

To obtain the sensitivity $\nabla_s f$ of Equation (27), by adding Equations (29) and (30) and by substituting Equation (32) into it, the equation is arranged as follows.

$$\begin{aligned}\nabla_s f &= -\boldsymbol{d}^{\mathrm{T}}\int_{\Omega^{\mathrm{b}}}(\nabla_s\boldsymbol{B}^{\mathrm{b}^{\mathrm{T}}})\mathbb{C}^{\mathrm{b}}_{\mathrm{G}}\boldsymbol{B}^{\mathrm{b}}\mathrm{d}\Omega^{\mathrm{b}}\boldsymbol{d} - \boldsymbol{d}^{\mathrm{T}}\int_{\Omega^{\mathrm{b}}} \boldsymbol{B}^{\mathrm{b}^{\mathrm{T}}}\left(\nabla_s\mathbb{C}^{\mathrm{b}}_{\mathrm{G}}\right)\boldsymbol{B}^{\mathrm{b}}\mathrm{d}\Omega^{\mathrm{b}}\boldsymbol{d} \\ &\quad - \boldsymbol{d}^{\mathrm{T}}\int_{\Omega^{\mathrm{b}}} \boldsymbol{B}^{\mathrm{b}^{\mathrm{T}}}\mathbb{C}^{\mathrm{b}}_{\mathrm{G}}(\nabla_s\boldsymbol{B}^{\mathrm{b}})\mathrm{d}\Omega^{\mathrm{b}}\boldsymbol{d} - \boldsymbol{d}^{\mathrm{T}}\int_{\Omega^{\mathrm{b}}} \boldsymbol{B}^{\mathrm{b}^{\mathrm{T}}}\mathbb{C}^{\mathrm{b}}_{\mathrm{G}}\boldsymbol{B}^{\mathrm{b}}(\nabla_s\mathrm{d}\Omega^{\mathrm{b}})\boldsymbol{d}.\end{aligned} \tag{33}$$

As the $\int_{\Omega^{\mathrm{b}}} \boldsymbol{B}^{\mathrm{b}^{\mathrm{T}}}\mathbb{C}^{\mathrm{b}}_{\mathrm{G}}\boldsymbol{B}^{\mathrm{b}}d\Omega^{\mathrm{b}}$ is a stiffness matrix $\boldsymbol{K}^{\mathrm{b}}$ of the rockbolts shown in Equation (15), the sensitivity of the objective function can be expressed as follows.

$$\nabla_s f = -\boldsymbol{d}^{\mathrm{T}}(\nabla_s\boldsymbol{K}^{\mathrm{b}})\boldsymbol{d} \tag{34}$$

$$= -\boldsymbol{d}^{\mathrm{T}}\nabla_s\boldsymbol{K}\boldsymbol{d}, \tag{35}$$

where $\nabla_s \boldsymbol{K}^{\mathrm{b}}$ is replaced by $\nabla_s \boldsymbol{K}$ simply to use the program to build a global stiffness matrix $\boldsymbol{K}$ by assembling stiffness matrices of embedded elements in structural analysis. As a matter of course, the differentiation of the local stiffness matrix of natural ground with respect to the design variable, introduced in Equation (15), is $\nabla_s \boldsymbol{K}^{\mathrm{r}} = \boldsymbol{0}$, and it does not affect the sensitivity produced by the aforementioned equation.

ACKNOWLEDGEMENT

This work was supported by MEXT KAKENHI Grant Numbers 23560561 and 23656285. This study partially employs an analyzing program, CCARAT, developed by University of Stuttgart, Germany. This support is gratefully acknowledged.

REFERENCES

1. Kato J. Material optimization for fiber reinforced composites applying a damage formulation. *Ph.D. dissertation*, Institute of Structural Mechanics, University of Stuttgart, Germany, 2010.
2. Kato J, Ramm E. Multiphase layout optimization for fiber reinforced composites considering a damage model. *Engineering Structures* 2013; **49**:202–220.
3. Balakrishnan S, Murray DW. Finite element prediction of reinforced concrete behavior. *Structural Engineering Report, No. 138*, University of Alberta, Edmonton, Alberta, Canada, 1986.
4. Barzegar F, Maddipudi S. Generating reinforcement in FE modeling of concrete structures. *Journal of Structural Engineering* 1994; **120**(5):1656–1662.
5. Chang TY, Taniguchi H, Chen WF. Nonlinear finite element analysis of reinforced concrete panels. *Journal of Structural Engineering, ASCE* 1987; **113**(1):122–140.
6. Elwi AE, Hrudey TM. Finite element model for curved embedded reinforcement. *Journal of Engineering Mechanics* 1989; **115**(4):740–754.
7. Hofstetter G, Mang HA. Work-equivalent node forces from prestress of concrete shells. In *Finite Element Methods for Plate and Shell Structures, Formulations and Algorithms*, Vol. 2, Hughes TJR, Hinton E (eds). Pineridge Press: Swansea, 1986; 312–347.
8. Phillips DV, Zienkiewicz OC. Finite element nonlinear analysis of concrete structures. *Proc. Institution of Civil Engineers, Part 2* 1976; **61**(3):59–88.
9. Svanberg K. The method of moving asymptotes – a new method for structural optimization. *International Journal for Numerical Methods in Engineering* 1987; **24**:359–373.
10. Svanberg K. A globally convergent version of MMA without linesearch. In *Proceedings of the First World Congress on Structural and Multidisciplinary Optimization, WCSMO-1*, Olhoff N, Rozvany GIN (eds): Goslar, Germany, 1995; 9–16.
11. Svanberg K. A class of globally convergent optimization methods based on conservative convex separable approximations. *SIAM Journal on Optimization* 2002; **12**(2):555–573.
12. Kato J, Lipka A, Ramm E. Multiphase material optimization for fiber reinforced composites with strain softening. *Structural and Multidisciplinary Optimization* 2009; **39**:63–81.
13. Kato J, Ramm E. Optimization of fiber geometry for fiber reinforced composites considering damage. *Finite Elements in Analysis and Design* 2010; **46**:401–415.
14. Bendsøe MP, Neves MM, Sigmund O. Some recent results on topology optimization of periodic composites. *Proceedings of the NATO Advanced Research Workshop on Topology Optimization of Structures and Composite Continua*, Budapest, Hungary, 2000; 3–17.
15. Zhou M, Rozvany GIN. The COC algorithm, part II: Topological, geometrical and generalized shape optimization. *Computer Methods in Applied Mechanics and Engineering* 1991; **89**:309–336.
16. Sigmund O, Torquato S. Design of materials with extreme thermal expansion using a three-phase topology optimization method. *Journal of the Mechanics and Physics of Solids* 1997; **45**(6):1037–1067.
17. Stolpe M, Stegmann J. A Newton method for solving continuous multiple material minimum compliance problems. *Structural and Multidisciplinary Optimization* 2008; **35**:93–106.

DOI: 10.1002/nag